THE INFLUENCE OF ROTATIONAL FRONTOGENESIS AND ITS ASSOCIATED SHEARWISE VERTICAL MOTIONS ON THE DEVELOPMENT OF AN UPPER-LEVEL FRONT

by

ANDREA A. LANG and JONATHAN E. MARTIN

Department of Atmospheric and Oceanic Sciences
University of Wisconsin-Madison
1225 W. Dayton Street
Madison, WI 53706
Ph. (608) 262-9845
Fax (608) 262-0166
jemarti1@wisc.edu

Submitted for publication to *Quarterly Journal of the Royal Meteorological Society*: August 27, 2009
Revised version submitted: October 1, 2009
Second revised version submitted: October 27, 2009

ABSTRACT

The total quasi-geostrophic (QG) vertical motion is partitioned into transverse and shearwise couplets oriented parallel to, and along, the geostrophic vertical shear, respectively, in order to examine the role of rotational frontogenesis, and its associated shearwise circulation, in the life cycle of an upper-front/jet system in northwesterly flow. In particular the analysis emphasizes two aspects of that role; 1) the influence of shearwise ω on scalar frontogenesis, and 2) the effect of rotational frontogenesis, and its associated vertical circulation, on the initiation of along-flow cold air advection during upper frontogenesis.

The case study analysis reveals that shearwise subsidence persistently and significantly contributes to scalar frontogenesis throughout the life cycle. The transverse subsidence contribution to scalar frontogenesis is initially weak but grows more substantial after the establishment of along-flow cold air advection near the base of the thermal trough.

Prior work has argued that the development of along-flow cold air advection arises from a cyclonic rotation of $\nabla\theta$ promoted either by contributions from tilting or horizontal kinematics. From the QG perspective adopted in the present study, the tilting and kinematic rotations are seen as interconnected aspects of a single, underlying dynamical process; rotational frontogenesis, in which the rotation of $\nabla\theta$ produced by vertical vorticity is accompanied by a discrete vertical circulation (the shearwise circulation) that provides the subsidence upshear of the vorticity maximum required to initiate along-flow cold air advection. It is further suggested that the characteristic distribution of the kinematic and tilting contributions to rotation of $\nabla\theta$ in the vicinity of an upper-tropospheric vorticity maximum underlies the observed preference for the development of upper-level fronts in northwesterly flow. KEYWORDS; *upper-level frontogenesis, partitioned **Q**-vectors, Shapiro effect, rotational frontogenesis*

1. Introduction

A distinguishing feature of the baroclinic wave life cycle is the development of narrow zones of enhanced temperature and momentum gradients known as frontal zones. Such zones are characterized by large density contrasts, enhanced static stability, local maxima in vertical vorticity, strong vertical wind shear, widths of order 100 km, and lengths of order 1000 km. Though baroclinic zones with these frontal properties can exist throughout the entire depth of the troposphere and lower stratosphere, they are particularly robust near the Earth's surface (surface fronts) where an impermeable solid boundary exists and at upper-levels (upper-level fronts) near the *thermodynamic* boundary represented by the tropopause.

A resurgence of research attention surrounding aspects of the life cycle of upper-level frontal zones has followed Keyser and Shapiro's (1986) comprehensive review of the first half century of work concerning the structure and dynamics of these features. From among the many topics discussed and questions raised therein, the nature of the vertical motions involved in upper-level frontogenesis, and the environments within which these vertical motions develop, are most germane to the present study. The Sawyer (1956)-Eliassen (1962) equation was the first diagnostic tool to explicitly make the connection between frontogenetic forcing (stretching and shearing deformation in geostrophic flow) and the production of the transverse ageostrophic circulation. Arguing from the Sawyer-Eliassen perspective, Shapiro (1981) suggested that the presence of cold air advection in cyclonic shear could strengthen the subsiding branch of the direct circulation in the confluent jet entrance region and shift it toward the warm side of an

upper baroclinic zone (i.e. what was later termed the Shapiro effect by Rotunno et al. (1994)). This suggestion was demonstrated in a 2D, primitive equation simulation by Keyser and Pecnick (1985) who found subsidence maximized beneath the jet core under such circumstances. Such a distribution of vertical motion is strongly upper-frontogenetical.

Considerable debate has ensued regarding the mechanisms by which cold air advection, central to the initiation of the frontogenetical Shapiro effect, develops in the vicinity of the maturing upper-level front. In fact, this question has been examined from both idealized modeling and observational perspectives. Rotunno et al. (1994) (hereafter RSS) analyzed normal mode cyclogenesis in a primitive equation channel model to examine the upper frontogenesis process in an atmosphere with a constant potential vorticity (PV) stratosphere. They considered the transition from a nearly equivalent barotropic environment, with little or no along-flow thermal advection in the upper troposphere, to an environment characterized by strong cold air advection near the base of an upper trough just a day later. They argued that the development of such along-flow cold air advection was initiated by subsidence maximized in northwesterly flow slightly downstream of the inflection between a ridge and downstream trough (i.e. upstream of a vorticity maximum). The along-flow increase in the strength of the subsidence, through its associated variations in adiabatic warming, induced a cyclonic rotation of the horizontal potential temperature gradient vector (hereafter $\nabla_h\theta$) which reoriented the isentropes relative to the isohypses and promoted the development of cold air advection. RSS did not relate this subsidence to any particular dynamical process.

In an observational study, Schultz and Doswell (1999) (hereafter SD) extended the 2D

vector frontogenesis formulation of Keyser et al. (1988) to include terms related to vertical tilting in order to consider the mechanism(s) underlying the initiation and distribution of along-flow cold air advection in an observed case of northwesterly flow upper-level frontogenesis[1]. They concluded that the rotation of $\nabla_h\theta$ associated with tilting was of second order importance compared to that associated with vertical vorticity. They were thus led to emphasize the role of horizontal winds in the rotation of isentropes and in the establishment of cold air advection near the base of the thermal trough[2]. Though vorticity rotates every vector field equally, and therefore cannot promote the *differential* rotation of $\nabla\theta$ relative to $\nabla\phi$ required to initiate along-flow *geostrophic* cold air advection, SD's analysis nonetheless suggested a primary role for rotational frontogenesis in the upper frontal life cycle.

The present paper examines a case of northwesterly flow upper frontogenesis in order to demonstrate that these seemingly disparate views may be interpreted as components of a single, underlying process by which along-flow cold air advection, and the frontogenetic Shapiro effect, develop during upper frontogenesis. The diagnostic tool by which this interpretation is advanced is the partitioned quasi-geostrophic (QG) $\boldsymbol{Q}$-vector approach first suggested by Keyser et al. (1988), and explored more thoroughly by Keyser et al. (1992). As will be shown later, this approach allows the discrete vertical circulations associated with changes in the magnitude and direction of $\nabla\theta$ (the so-called scalar and rotational frontogenesis, respectively) to be isolated.

---

[1] They also considered a case of the less studied southwesterly flow upper-level frontogenesis from this perspective and found that increasing cold air advection along the front was related to an upstream vorticity maximum in both cases.

[2] A similar conclusion with regard to this question, based upon examination of a thermal advection tendency equation, was reached by Schultz and Sanders (2002).

The analysis will show that the rotational frontogenesis (highlighted by SD) is accompanied by a vertical circulation that provides the subsidence upshear of the vorticity maximum (highlighted by RSS) required to initiate along-flow cold air advection.

The paper is structured in the following manner. Section 2 provides a description of vector frontogenesis and its QG equivalent which leads directly to the method of partitioning QG omega. Section 3 provides a synoptic overview of the upper-front of interest. Analysis of the QG vertical motion associated with the evolution of the upper-front is presented in Section 4. Section 5 provides analysis and discussion of the results, offers a summary, and points to future work.

2. Vector frontogenesis and vertical motion

Keyser et al. (1988) provided a generalization of the Petterssen (1936) frontogenesis equation, by examining the Lagrangian rate of change of the *magnitude* and *direction* of the horizontal potential temperature gradient vector,

$$\boldsymbol{F} = \frac{d}{dt_h}\nabla_h\theta. \qquad (1)$$

In their formulation, they considered the effect of the horizontal wind only, so that $\frac{d}{dt_h} = \frac{\partial}{\partial t} + u\frac{\partial}{\partial x} + v\frac{\partial}{\partial y}$. Keyser et al. (1988) exploited this conceptual extension of $\boldsymbol{F}$ by considering components using a natural coordinate system, defined by the local orientation of the isentropes in the horizontal plane such that $\hat{n}$ was directed across the isentropes toward colder air

and $\hat{s}$ was 90° clockwise of $\hat{n}$. In such a coordinate frame, $\boldsymbol{F} = F_n \hat{n} + F_s \hat{s}$. Frontogenetic forcing in the $\hat{n}$ direction was referred to as *scalar* frontogenesis or F_n and is equal to

$$F_n = -\frac{|\nabla\theta|}{2}[E\cos 2\beta - D] \qquad (2a)$$

where E is the total deformation, D is the divergence and β is the angle between the isentropes and the axis of dilatation of the total deformation field. This type of forcing is associated with a modification of the *magnitude* of the potential temperature gradient and is equivalent to Petterssen's frontogenesis equation (note that $F_n < 0$ describes frontogenesis). Frontogenetic forcing in the $\hat{s}$ direction was referred to as *rotational* frontogenesis or F_s, and is equal to

$$F_s = \frac{|\nabla\theta|}{2}[E\sin 2\beta + \zeta] \qquad (3a)$$

where ζ is the vertical vorticity. This type of forcing results in a modification of the *direction* of the potential temperature gradient vector.

Noting the importance of vertical motions in the life cycle of upper-level fronts, SD extended Keyser et al's (1988) methodology to include the frontogentical effects of vertical motions. Accordingly, they derived expressions for the rates of change of the magnitude and direction of the *horizontal* potential temperature gradient following the *3-D* wind. The natural coordinate components of the resulting expression

$$\boldsymbol{F} = \frac{d}{dt}\nabla_h\theta = F_n\hat{n} + F_s\hat{s}$$

are

$$F_n = -\frac{|\nabla\theta|}{2}[E\cos 2\beta - D] - \frac{\partial\theta}{\partial p}\frac{\partial\omega}{\partial n} \qquad (2b)$$

and

$$F_s = \frac{|\nabla\theta|}{2}[E\sin 2\beta + \zeta] - \frac{\partial\theta}{\partial p}\frac{\partial\omega}{\partial s}. \qquad (3b)$$

Taking up the suggestion made by Keyser et al. (1988), who noted that the so-called $\boldsymbol{Q}$ vector, introduced by Hoskins et al. (1978), was the QG form of (1), Keyser et al. (1992) applied the quasi-geostrophic (QG) assumption to $\boldsymbol{F}$. Exploiting the fact that for horizontal adiabatic flow,

$$\boldsymbol{Q} = \frac{d}{dt_g}\nabla_p\theta \qquad (4)$$

where $\frac{d}{dt_g} = \frac{\partial}{\partial t} + u_g\frac{\partial}{\partial x} + v_g\frac{\partial}{\partial y}$ and p represents differentiation on a constant pressure surface, they employed a similar natural coordinate partitioning of $\boldsymbol{Q}$ where $\boldsymbol{Q} = Q_n\hat{n} + Q_s\hat{s}$. The across (along) isentrope component of $\boldsymbol{Q}$, $\boldsymbol{Q_n} = Q_n\hat{n}$ ($\boldsymbol{Q_s} = Q_s\hat{s}$) describes the rate of change of the *magnitude* (*direction*) of $\nabla\theta$ following the geostrophic wind.[3]

Since the QG omega equation

$$\sigma(\nabla^2 + \frac{f_o^{\,2}}{\sigma}\frac{\partial^2}{\partial p^2})\omega = -2\nabla\cdot\boldsymbol{Q} \qquad (5)$$

describes the vertical motion (ω) forced by the divergence of the QG equivalent of $\boldsymbol{F}$ (the $\boldsymbol{Q}$ vector), it follows that the divergences of $\boldsymbol{Q}$, $\boldsymbol{Q_n}$, and $\boldsymbol{Q_s}$ return the total (ω_{tot}), transverse (ω_n), and shearwise (ω_s) QG vertical motions, respectively. Thus, this framework allows the vertical circulation associated with rotational frontogenesis (what Martin (2006) termed the *shearwise* ω) to be isolated and its effects on aspects of the development of an upper-level front to be examined. Motivated by a desire to develop a more comprehensive understanding of the role of

[3] Note that Q_n (Q_s) is the geostrophic equivalent of F_n (F_s). When $\boldsymbol{Q_s}$ is directed along (opposite)

rotational frontogenesis in the development of upper-level frontal zones, the present paper particularly considers two such aspects; 1) the contribution of shearwise ω to scalar frontogenesis via the tilting term, the last term in (2b), and 2) the effect of rotational frontogenesis, and its associated vertical circulation, on the initiation of along-flow cold air advection during upper frontogenesis. As the study focuses on the life cycle of a characteristic northwesterly flow upper-level front over central North America, the analysis begins with a synoptic overview of that feature.

3. Synoptic evolution of the upper front

At 1200 UTC 11 November 2003, a high amplitude flow pattern over North America was evident as a strongly baroclinic northwesterly flow entered the northwestern United States (Fig. 1a). At 400 hPa this baroclinic zone contained a strip of vorticity oriented along the isentropes from extreme southeastern Alaska to Washington. Downstream of the Pacific Northwest, the baroclinic zone weakened. Another noteworthy feature of the flow was the dominant positively tilted shortwave trough that stretched southwestward from southwestern Wyoming across the California coast into the Pacific Ocean. The upper-level flow over the United States was characterized by a second baroclinic zone that originated downstream of the axis of this shortwave and stretched northeastward over the Rockies to the Great Lakes region (Fig. 1a). The jet associated with this shortwave possessed winds exceeding 70 m s^{-1} over the central Plains (Fig. 1b). At this time, the polar jet was oriented nearly perpendicularly to the sub-tropical jet,

---

the geostrophic vertical shear, cyclonic (anticyclonic) rotation of $\nabla\theta$ is implied.

and was also a fairly linear feature with a maximum speed of 70 m s^{-1} over southeastern Alaska (Fig. 1b). Geostrophic temperature advection at 400 hPa along the northwesterly flow baroclinic zone was uniformly positive at this time (Fig. 1c).

By 0000 UTC 12 November, the northern 400 hPa shortwave, located at the left exit region of the polar jet, had shifted slightly eastward as had its associated baroclinic zone (Fig. 2a). The southern extremity of this developing upper-front reached further south than at the previous time, extending into southwestern Wyoming. The 400 hPa thermal trough had also amplified by this time, with its axis stretching from central Alberta, through central Montana, into Wyoming. At 300 hPa the northwesterly jet axis was also oriented more or less along the isentropes that defined the upper-front. The maximum wind speed, centered over the British Columbia-Alberta border, had decreased to just over 60 m s^{-1} (Fig. 2b). This jet exhibited an abrupt exit region, situated near the Idaho-Wyoming border, where the flow joined the northwestern edge of the southwesterly sub-tropical jet along the front range of the Rocky Mountains. The 400 hPa geostrophic temperature advection along the polar jet was, as before, uniformly positive to the west of the thermal and geopotential height trough axes (Fig. 2c).

By 1200 UTC 12 November the upper-level front had intensified from Alberta southward into the northern Plains of the United States where it reached the base of the geopotential height trough over the South Dakota/Nebraska border. The strongest portion of the front was centered on the eastern border of Wyoming, where the potential temperature gradient was ~5.25 K $(100\ km)^{-1}$ (Fig. 3a). At 300 hPa, the abrupt exit region of the northwesterly jet weakened. The flow joined the southwesterly jet streak, creating a meandering polar jet which

had several speed maxima of over 60 m s^{-1} scattered across northern Alberta, the central Plains, and the southern Great Lakes regions (Fig. 3b). During the intervening 12 h substantial geostrophic cold air advection, centered over northwestern Nebraska, had developed at the base of the 400 hPa thermal trough (Fig. 3c).

By 0000 UTC 13 November the upper-front stretched from the northern Plains to the Great Lakes region where it emerged in the southwesterly flow over lower Michigan (Fig. 4a). The magnitude of the potential temperature gradient (~ 8 K (100 km)$^{-1}$ along the eastern border of Iowa) reached its peak at this time. The absolute vorticity at 400 hPa was oriented in a strip along the upper-front, with a local maximum at the eastern edge of the frontal zone (Fig. 4a). The 300 hPa jet streak centered over southern Iowa continued to intensify, reaching speeds of over 80 m s^{-1} by this time (Fig. 4b). The jet axis was oriented along the warm side of the upper-front with stronger geostrophic cold air advection through the jet core (Fig. 4c) than at any prior time. After this time, the upper-front became a component of a troposphere-deep frontal structure associated with the cyclogenesis event described by Martin (2006).

4. Quasi-Geostrophic Vertical Motion

In this section, gridded model analyses from the National Centers for Environmental Prediction's (NCEP's) Eta model (Eta 104-grid) are used in the calculation of QG omega and its components. These gridded data are first bilinearly interpolated from their original output grid to a 1°x1° latitude–longitude grid at 19 isobaric levels (from 1000 to 100 hPa at 50 hPa intervals)

using an interpolation program included in the General Meteorological Analysis Package (GEMPAK). The gridpoint height and temperature data are then subjected to a Gaussian smoother that eliminates roughly 2/3 of the energy at wavelengths ≤ 660 km, yielding results similar to those achieved using the cowbell filter described by Barnes et al. (1996) for use in quasi-geostrophic diagnostics with meso-scale models. Employing the technique of successive over relaxation (SOR), we then solve the *f*-plane version of the QG omega equation using a spatially averaged static stability that varies for each time with f_o set equal to the central latitude (45.5°N) of the domain for this case. With geostrophic forcing corresponding to the divergences of $\boldsymbol{Q}$, $\boldsymbol{Q_n}$, and $\boldsymbol{Q_s}$, the total (ω_{tot}), transverse (ω_n), and shearwise (ω_s) QG vertical motions, respectively, are returned in units of Pa s^{-1}. As noted by Martin (1998), since $\hat{n}$ and $\hat{s}$ change direction along isentropes, $\nabla \cdot \hat{n}$ and $\nabla \cdot \hat{s}$ can contribute to $\nabla \cdot \vec{Q}_n$ and $\nabla \cdot \vec{Q}_s$, respectively. Calculation of this effect (not shown) revealed that the unit vector contribution to $\boldsymbol{Q}$ divergence was negligible in this case. The subsequent analysis centers on the evolution of QG omega and the tilting frontogenesis at both the 400 hPa level and in vertical cross sections corresponding to the time periods analyzed in Section 3. Since the tilting frontogenesis is given by $-\frac{\partial \theta}{\partial p}\frac{\partial \omega}{\partial n}$ (i.e the last term in (2b)), we shall separately refer to the total, shearwise, and transverse tilting frontogenesis calculated using the ω_{tot}, ω_s, and ω_n, respectively.

The 400 hPa total QG vertical motion field along with the total tilting frontogenesis at 1200 UTC 11 November is shown in Fig. 5a. The northwesterly flow baroclinic zone was characterized by several pockets of subsidence along the Canadian west coast (Fig. 5a) that

combined to produce a nearly continuous swath of positive tilting frontogenesis on the cold (i.e. cyclonic shear) side of the upper baroclinic zone throughout British Columbia. At the southern end of the baroclinic zone, ascent was located from eastern Washington to southern Alberta and the isentropes fanned out immediately downstream of this region. In the partitioned omega fields, pockets of shearwise omega captured nearly all of the full QG vertical motion in the northwesterly flow (Fig. 5b). Correspondingly, the shearwise tilting frontogenesis (Fig. 5b) is very similar to the total tilting frontogenesis shown in Fig. 5a. Meanwhile, the transverse omega contributed very little to the full QG omega in the vicinity of the upper-front (Fig. 5c) and correspondingly meager transverse tilting frontogenesis. The relatively strong couplet of shearwise omega located over southern British Columbia and Washington state (Fig. 5b) was related to $\boldsymbol{Q_s}$ vectors that were associated with positive rotational frontogenesis and a corresponding counterclockwise rotation of the isentropes along that portion of the baroclinic zone.

Several cross-sections perpendicular to the upper-front at this time (along the line A-A' in Fig. 5a) were constructed. The total QG omega along this line, illustrated in Fig. 6a, shows subsidence between 325 hPa and 800 hPa, with a maximum centered at approximately 475 hPa, slightly on the warm side of the baroclinic zone beneath the jet core. This distribution contributed to intensification of the upper-front via total tilting frontogenesis from the level of maximum winds to ~600 hPa on the cyclonic shear side of the jet. Nearly all of the differential subsidence across the baroclinic zone, and the resulting tilting frontogenesis, was accounted for by the shearwise component of vertical motion and its attendant shearwise tilting frontogenesis

(Fig. 6b), as the transverse vertical motion contributed very little (Fig. 6c).

At 0000 UTC 12 November, subsidence continued to dominate the total QG vertical motion in the northwesterly flow as the upper-front intensified (Fig 7a). The southern portion of the frontal zone, located from the Montana/Alberta border to central Wyoming, was characterized by the largest subsidence with three local maxima on the warm side of the front contributing to dramatically larger tilting frontogenesis than had been seen earlier. The $\boldsymbol{Q}_s$ vectors along this portion of the frontal zone were associated with continued positive rotational frontogenesis (Fig. 7b). The corresponding shearwise omega field (Fig. 7b), though contributing the largest share of the total descent, was not the dominant frontogenetic factor at this time, as the transverse omega played an equal role in forcing warm side subsidence along this portion of the front by this time (Fig. 7c). In fact, the linear nature of the total tilting frontogenesis there (Fig. 7a) was largely a function of the transverse tilting frontogenesis.

Several vertical cross-sections perpendicular to the upper-front at this time (along line B-B' in Fig. 7a) are shown in Fig. 8. These sections cut through the northern region of maximum subsidence within the upper frontal zone. QG subsidence characterized the entire depth of the troposphere beneath the jet core, with a local maximum between 600 to 300 hPa within the upper-front (Fig. 8a). The resulting total tilting frontogenesis was strong between the jet-level and ~550 hPa on the cyclonic shear side of the jet core. Shearwise omega was responsible for the majority of the subsidence along this cross-section line, and roughly half of the total tilting frontogenesis, throughout the depth of the troposphere (Fig. 8b). The small patch of transverse subsidence located on the warm side of the upper-front, with a maximum centered at

approximately 400 hPa, was in a position where it too contributed to the thermally indirect circulation that promoted upper frontogenesis on the cyclonic shear side of the jet (Fig. 8c).

The distribution of vertical motion at 1200 UTC 12 November was characterized by an amplified region of subsidence on the warm edge of the frontal zone on the Montana/Wyoming border (Fig. 9a) This subsidence, with a magnitude of approximately 12 dPa s^{-1}, and a region of weak ascent downstream of the upper-front, formed a couplet that straddled the base of thermal trough in the northern Plains. Associated with this strong subsidence was extremely strong total tilting frontogenesis (more than twice the magnitude recorded at 0000 UTC 12 November) along an axis from southeastern Montana to northeastern Nebraska. The $\boldsymbol{Q_s}$ vectors were large and in the direction of the thermal wind in the base of the thermal trough, illustrating the substantial positive rotational frontogenesis that continued along the southern extent of the frontal zone. The corresponding shearwise omega was largely responsible for the couplet of vertical motion and continued to contribute the majority of vertical motion associated with the developing upper-front (Fig. 9b). However, the contribution by the transverse omega continued to increase, with a band of subsidence oriented along and to the warm side of the most intense portion of the upper-front from southeastern Montana to southeastern Nebraska (Fig. 9c) which contributed to strong transverse tilting frontogenesis from southeastern Montana through South Dakota. The shearwise tilting frontogenesis was nearly coincident, of comparable magnitude nearly everywhere and of greater magnitude in southeastern Montana (Fig. 9b).

Vertical cross sections just upstream of the thermal trough at this time are shown in Fig. 10. The ω_{tot} maximum toward the warm side of the frontal zone was responsible for significant

total tilting frontogenesis on the cyclonic shear side of the jet from ~250 to 600 hPa (Fig. 10a). Roughly 60% of the total tilting frontogenesis was accounted for by the shearwise tilting frontogenesis (Fig. 10b) with the remainder contributed by the weaker transverse tilting frontogenesis (Fig. 10c).

By 0000 UTC 13 November the magnitude of total QG ascent downstream of the upper-front surpassed the magnitude of total QG subsidence within the upper-front (Fig. 11a) which had weakened substantially in the twelve hour period, to approximately 10 dPa s^{-1}. The associated total tilting frontogenesis had weakened in the same interval yet continued to display a similar distribution relative to the frontal zone as it had 12 h previously. Strong ascent, roughly 18 dPa s^{-1}, was associated with rapid surface cyclogenesis over the eastern Great Lakes, as described by Martin (2006). This pocket of ascent was primarily shearwise omega (Fig. 11b) with some contribution from the transverse ascent (Fig. 11c), located in the left exit region of the jet streak. The total QG subsidence was composed of a shearwise contribution along the South Dakota/Nebraska border (Fig. 11b) and a broad band of predominantly transverse subsidence stretching from southern Manitoba to Illinois (Fig. 11c). It was this subsidence and its associated transverse tilting frontogenesis that dictated the overall linear nature of the total tilting frontogenesis at this time.

Vertical cross sections of tilting frontogenesis near the base of the thermal trough at this time are shown in Fig. 12. Total tilting frontogenesis remained strong from the level of maximum winds to ~600 hPa (Fig. 12a). The contributions from shearwise and transverse tilting frontogenesis were nearly identical at this time, especially in the upper troposphere on the cyclonic shear side of the jet (Figs. 12b,c). The thermally direct transverse couplet below 550 hPa (Fig. 12c) attended near surface frontal intensification associated with rapid cyclogenesis

that was occurring over the eastern Great Lakes (Martin 2006).

5. Discussion and Conclusions

In this paper the partitioned QG omega perspective has been employed to examine the role of rotational frontogenesis on the development of an upper-level front in northwesterly flow. In particular, the analysis has emphasized two aspects of that role; 1) the contribution of shearwise ω to scalar frontogenesis, and 2) the effect of rotational frontogenesis, and its associated vertical circulation, on the initiation of along-flow cold air advection during upper frontogenesis.

Though SD established the importance of rotational frontogenesis to upper frontogenesis, they were not able to explicitly consider the role that the secondary vertical circulation associated with the rotational frontogenesis might play in the intensification of an upper-level front. The scalar frontogenesis function employed here is that derived by SD to account for the rate of change of the magnitude of the horizontal potential temperature gradient following the 3-D wind (eq. 2b). Our analysis of the separate contributions made by ω_{tot}, ω_s, and ω_n to the tilting scalar frontogenesis (e.g. $-\frac{\partial\theta}{\partial p}\frac{\partial\omega}{\partial n}$, the last term in (2b)) suggests that a substantial share (the largest share throughout most of this upper-front life cycle) was contributed by the shearwise subsidence. As the upper-front intensified and along-flow cold air advection developed near and upshear of the base of the thermal trough, the transverse tilting acquired larger magnitude and exerted a greater control on the linear geometry of the evolving frontal zone.

Though upper-level fronts are known to develop in both northwesterly and

southwesterly flow, the most intense upper frontogenesis events take place in northwesterly flow where the primary intensification mechanism is differential subsidence (p. 2536, Schultz and Doswell 1999). A particularly favorable synoptic environment within which northwesterly flow upper frontogenesis occurs is one characterized by cold air advection in cyclonic shear. A number of modeling studies based on observed and idealized flows (i.e. Shapiro 1981, Keyser and Pecnick 1985, Keyser et al. 1986, Reeder and Keyser 1988, Rotunno et al. 1994) have shown that cold air advection in cyclonic shear promotes the establishment of a thermally indirect transverse circulation capable of scalar frontogenetic tilting and upper frontogenesis. In most observed cases of northwesterly flow upper frontogenesis, however, cold air advection does not occur along the entire length of the developing front. In fact, the majority of cases described in the literature exhibit mixed thermal advection along their lengths; cold air advection near the base of the thermal trough but often warm air advection some distance upstream of the thermal trough (Schultz and Doswell 1999). In the present case the thermal advection was nearly entirely positive early in the upper front life cycle (Figs. 1c, 2c) with cold air advection developing and becoming further concentrated near the base of the thermal trough as the development proceeded (Figs. 3c, 4c). As the cold air advection intensified, so did the contribution of the transverse subsidence to upper frontogenesis as illustrated by consideration of Figs. 6c, 8c, 10c, and 12c. Thus, the mechanism that leads to the initiation and distribution of cold air advection near the base of the thermal trough is an important aspect of the upper frontogenesis process.

Rotunno et al. (1994) analyzed normal mode cyclogenesis in a baroclinic primitive equation channel model to examine the northwesterly flow upper frontogenesis process and

mechanisms for the onset of along-front cold air advection. Their analysis focused on subsiding cold air in northwesterly flow between an upstream ridge and downstream trough as the primary mechanism for establishing cold air advection in cyclonic shear. Further clarification concerning the role of subsidence in this regard arises from the analysis of SD who showed that an along-isentrope increase in subsidence (i.e. $\frac{\partial \omega}{\partial s} > 0$) promotes cyclonic rotation of $\nabla\theta$ through the tilting contribution to F_s ($-\frac{\partial \theta}{\partial p}\frac{\partial \omega}{\partial s}$), though they considered this of secondary importance and concluded that the primary mechanism for establishing cyclonic rotation of $\nabla\theta$ was provided, kinematically, by the vorticity field itself.

In the face of such different emphases, it is instructive to consider the fact that the environment surrounding a vorticity maxima in shear flow can be conceptually divided into three regions; one upshear of the maxima, one downshear of the maxima, and one encompassing the maxima as shown schematically in Fig. 13. The Sutcliffe (1947)/Trenberth (1978) approximation to the QG ω-equation[4] diagnoses the characteristic distribution of vertical motions in this environment with a subsidence (ascent) maximum upshear (downshear) of the vorticity maximum as illustrated. Thus, in the regions upshear and downshear of the vorticity maximum, $\frac{\partial \omega}{\partial s} > 0$ and a cyclonic rotation of $\nabla\theta$ by tilting is implied via the last term in (3b). In the region encompassing the vorticity maxima, however, $\frac{\partial \omega}{\partial s} < 0$ and anticyclonic rotation via tilting is

[4] Martin (1999) showed that the Sutcliffe (1947)/Trenberth(1978) approximation actually describes twice the effect of the geostrophic relative vorticity on the rotation of $\nabla\theta$.

implied. Given that $\left|\frac{\partial \omega}{\partial s}\right|$ is smaller upshear and downshear of the vorticity maximum than it is in the vicinity of the vorticity maximum, the amount of rotation of $\nabla\theta$ provided by tilting in the upshear and downshear regions is smaller than that provided by tilting in the vicinity of the vorticity maxima. Furthermore, SD demonstrated that the cyclonic rotation of $\nabla\theta$ provided by the vertical vorticity in the vicinity of the vorticity maximum is larger in magnitude than the opposing tendency provided by the tilting. Therefore, the total rotational frontogenesis is largest near the vorticity maximum where cyclonic rotation by vorticity far exceeds anticyclonic rotation via tilting. Were the schematic vorticity maxima in Fig. 13 embedded within an upper trough axis, the upshear (downshear) region would be characterized by northwesterly (southwesterly) flow and parcels flowing *toward* the vorticity maxima (i.e. toward the trough axis in northwesterly flow) would experience a systematic *increase* in the forcing for cyclonic rotation of $\nabla\theta$; whereas quite the opposite would apply to those parcels streaming *away* from the vorticity maxima in southwesterly flow. This characteristic distribution of the kinematic and tilting contributions to rotational frontogenesis suggests that the development of cold air advection in cyclonic shear is preferred in northwesterly flow, resulting in more intense and more frequent upper frontogenesis under such circumstances.

The seemingly contradictory views of RSS and SD regarding the establishment of cold air advection and the frontogenetical Shapiro effect may now be reconciled. RSS emphasized the importance of subsidence maximized downstream of the northwesterly flow inflection point between a ridge and downstream trough as central to instigating the cyclonic rotation of $\nabla\theta$ near

and upstream of the base of the trough. Such a subsidence maximum is apparent in Figs. 7b, 9b, and 11b. SD emphasized the kinematic influence of the vorticity maximum itself on rotation of $\nabla\theta$. Such an influence is manifest in the $\boldsymbol{Q}_s$ vectors shown in Figs. 7b, 9b, and 11b which imply cyclonic rotation of $\nabla\theta$ at the location of the vorticity maximum. Since the strongest rotation will occur coincident with the largest $\boldsymbol{Q}_s$ vectors, there must be $\boldsymbol{Q}_s$ divergence (convergence) upshear (downshear) of that location. Thus, the shearwise subsidence maxima located upstream of the trough axis in Figs. 7b, 9b, and 11b is the sinking branch of the vertical circulation associated with the rotational frontogenesis. Consequently, the subsidence emphasized by RSS and the kinematic rotation emphasized by SD are interconnected aspects of a single, underlying dynamical process; rotational frontogenesis.

A synthesis of prior results with the present analysis suggests that rotational frontogenesis contributes to upper-level frontogenesis in the following ways. First, as demonstrated by SD, the rotational frontogenesis provides forcing for cyclonic rotation of $\nabla\theta$ near the base of the geopotential trough (more generally the relative vorticity maximum). Second, as shown here, the rotational frontogenesis is itself associated with a vertical circulation (the shearwise circulation) that provides the upshear subsidence maximum that initiates along-flow cold air advection as suggested by RSS. Thirdly, the shearwise subsidence persistently and significantly contributes to frontogenetic tilting. The superposition of the transverse and shearwise subsidence maxima, associated with the Shapiro effect and the rotational frontogenesis that spawns the Shapiro effect, respectively, led to a period of rapid upper frontogenesis in the present case. Whether or not the set of circumstances outlined here is characteristic of the life cycle of upper tropospheric jet/front systems is an outstanding question.

The dominant influence of the shearwise ω in the early stages of northwesterly flow upper frontogenesis in the present analysis, in terms of both the tilting frontogenesis and the initiation of cold air advection at the base of the thermal trough, is reminiscent of the primacy of shearwise updrafts in the cyclogenetic stage of the extratropical cyclone life cycle as described by Martin (2006, 2007). In those studies, as in this one, the contributions of the transverse vertical motions to the processes in question gradually increased as frontal structures began to take shape. This similarity suggests that the shearwise vertical motions, what Keyser et al. (1992) referred to as wave scale vertical motions, and the associated process of rotational frontogenesis play a primary role in molding the large scale flow into some of the basic synoptic scale structures involved in the production of sensible weather in the extratropics.

REFERENCES

Barnes, S. L., F. Caracena, and A. Marroquin, 1996: Extracting synoptic-scale diagnostic information from mesoscale models: The Eta model, gravity waves, and quasigeostrophic diagnostics. *Bull. Amer. Meteor. Soc*., **77**, 519-528.

Eliassen, A., 1962: On the vertical circulation in frontal zones. *Geofys. Publ.*, **24**(4), 147-160.

Hoskins, B. J., I. Draghici, and H. C. Davies, 1978: A new look at the ω-equation. *Quart. J. Roy. Meteo. Soc*., **104**, 31-38.

Keyser, D. and M. J. Pecnick, 1985: A two-dimensional primitive equation model of frontogenesis forced by confluence and horizontal shear. *J. Atmos. Sci.*, **42**, 1259-1282.

_____ and M. A. Shapiro, 1986: A review of the structure and dynamics of upper-level frontal zones. *Mon. Wea. Rev.,* **114**, 452-499.

_____, M. J. Reeder, and R. J. Reed, 1988: A generalization of Petterssen's frontogenesis function and its relation to the forcing of vertical motion. *Mon. Wea. Rev.* **116**, 762-780.

_____, B. D. Schmidt and D. G Duffy, 1992: Quasigeostrophic vertical motions diagnosed from along- and cross-isentrope components of the ***Q*** vector. *Mon. Wea. Rev.,* **120(**5), 731–741.

Martin, J. E., 1999: Quasigeostrophic forcing of ascent in the occluded sector of cyclones and the trowal airstream. *Mon. Wea. Rev.* **127**, 70-88.

_____, 2006: The role of shearwise and transverse quasigeostrophic vertical motions in the midlatitude cyclone life cycle. *Mon. Wea. Rev.* **134**, 1174–1193.

_____, 2007: Lower-tropospheric height tendencies associated with the shearwise and transverse components of quasigeostropic vertical motion. *Mon. Wea. Rev.* **135**, 2803–2809.

Petterssen, S., 1936: Contribution to the theory of frontogenesis. *Geofys. Publ.*, **11**(6), 1-27.

Reed. R. J., 1955: A study of a characteristic type of upper-level frontogenesis. *J. Meteor.*, **12**, 226-237.

_____ and F. Sanders, 1953: An investigation of the development of a mid-tropospheric frontal zone and its associated vorticity field. *J. Meteor.*, **10**, 338-349.

Reeder, M. J. and D. Keyser, 1988: Balanced and unbalanced upper-level frontogenesis. *J. Atmos. Sci.* **45(**22), 3366–3386.

Rotunno, R., W. C. Skamarock, and C. Snyder, 1994: An analysis of frontogenesis in numerical simulations of baroclinic waves. J. Atmos. Sci., 51, 3373-3398.

Sawyer, J. S., 1956: The vertical circulation at meteorological fronts and its relation to frontogenesis. *Proc. Roy. Soc. London*, **A234**, 346-362.

Schultz, D. M. and C. A. Doswell, 1999: Conceptual models of upper-level frontogenesis in south-westerly and north-westerly flow. *Quart. J. Roy. Meteor. Soc*, **125**, 2535-2562.

_____, and F. Sanders, 2002: Upper-level frontogenesis associated with the birth of mobile troughs in northwesterly flow. *Mon. Wea. Rev*., **130**, 2593-2610.

Shapiro, M. A., 1981: Frontogenesis and geostrophically forced secondary circulations in the vicinity of jet stream-frontal zone systems. *J. Atmos. Sci.*, **38**, 954-973.

Sutcliffe, R. C., 1947: A contribution to the problem of development. Quart. J. Roy. Meteor. Soc., 73, 370-383.

Trenberth, K. E., 1978: On the interpretation of the quasigeostrophic omega equation. *Mon. Wea. Rev*., **106**, 1321-137.

FIGURE CAPTIONS

Fig. 1 (a) 400 hPa geopotential height (solid lines), potential temperature (dashed) and absolute vorticity (shading) from the Eta model analysis valid at 1200 UTC 11 November 2003. Geopotential height is labeled in m and contoured every 120 m. Isentropes are labeled in K and contoured every 4 K. Absolute vorticity shown in units of 10^{-5} s^{-1} and shaded every 5 x 10^{-5} s^{-1} beginning at 15 x 10^{-5} s^{-1}. (b) 300 hPa geopotential height (solid lines) and isotachs (shaded) from the Eta model analysis valid at 1200 UTC 11 November 2003. Geopotential height labeled as in Fig. 1a and contoured every 200 m. Isotachs shown in m s^{-1} and shaded every 10 m s^{-1} beginning at 40 m s^{-1}. (c) 400 hPa geopotential height (solid lines), isentropes (dashed lines) and geostrophic temperature advection (shading) from the Eta model analysis valid at 1200 UTC 11 November 2003. Geopotential height labeled and contoured as in Fig. 1a. Isentropes labeled in K and contoured every 3K. Dark (light) shading represents negative (positive) geostrophic temperature advection in units of K s^{-1}, contoured every –2 (2) x 10^{-4} K s^{-1} beginning at –2 (2) x 10^{-4} K s^{-1}.

Fig. 2 (a) As for Fig. 1a but from the Eta model analysis valid at 0000 UTC 12 November 2003. (b) As for Fig. 1b but from the Eta model analysis valid at 0000 UTC 12 November 2003. (c) As for Fig. 1c but from the Eta model analysis valid at 0000 UTC 12 November 2003.

Fig. 3 (a) As for Fig. 1a but from the Eta model analysis valid at 1200 UTC 12 November 2003. (b) As for Fig. 1b but from the Eta model analysis valid at 1200 UTC 12 November 2003. (c) As for Fig. 1c but from the Eta model analysis valid at 1200 UTC 12 November 2003.

Fig. 4 (a) As for Fig. 1a but from the Eta model analysis valid at 0000 UTC 13 November 2003.

(b) As for Fig. 1b but from the Eta model analysis valid at 0000 UTC 13 November 2003.

(c) As for Fig. 1c but from the Eta model analysis valid at 0000 UTC 13 November 2003.

Fig. 5 (a) 400 hPa isentropes, $\boldsymbol{Q}$-vectors, total QG vertical motions (ω_{tot}), and total tilting frontogenesis from the Eta model analysis valid at 1200 UTC 11 November 2003. Thin solid lines are isentropes, labeled in K and contoured every 3K. Thick solid (dashed) lines are positive (negative) ω_{tot} contoured every 2 (-2) dPa s^{-1} beginning at 2 (-2) dPa s^{-1}. Tilting frontogenesis is in units of K m^{-1} s^{-1} and contoured every 8 (-8) x 10^{-10} K m^{-1} s^{-1} starting at 8 (-8) x 10^{-10} K m^{-1} s^{-1} with dark (light) shading indicating positive (negative) tilting frontogenesis. Vertical cross-sections along line A-A` shown in Fig. 6.

(b) As for Fig. 5a but with $\boldsymbol{Q_s}$ vectors, shearwise QG vertical motions (ω_s), and shearwise tilting frontogenesis from the Eta model analysis valid at 1200 UTC 11 November 2003. Tilting frontogenesis contoured in units of 4 (-4) x 10^{-10} K m^{-1} s^{-1} beginning at 4 (-4) x 10^{-10} K m^{-1} s^{-1}.

(c) As for Fig. 5a but with $\boldsymbol{Q_n}$ vectors, transverse QG vertical motions (ω_n), and transverse tilting frontogenesis from the Eta model analysis valid at 1200 UTC 11 November 2003. Tilting frontogenesis contoured and shaded as in Fig. 5b.

Fig. 6 (a) Vertical cross section, along line A-A` in Fig. 5a, of isotachs, isentropes, ω_{tot}, and total tilting frontogenesis from the Eta model analysis valid at 1200 UTC 11 November 2003. Thin dashed lines are isotachs labeled in m s^{-1} and contoured every 10 m s^{-1} starting at 40 m s^{-1}. Uppercase "J" indicates the location of the jet core. Isentropes

labeled and contoured as in Fig. 5a. Thick solid (dashed) lines are positive (negative) ω_{tot} labeled in dPa s^{-1} and contoured every 2 (-2) dPa s^{-1} beginning at 2 (-2) dPa s^{-1} but including the 1 (-1) dPa s^{-1} contour as well. Positive (negative) tilting frontogenesis is darkly (lightly) shaded and contoured every 3 (-3) x 10^{-10} K m^{-1} s^{-1} beginning at 3 (-3) x 10^{-10} K m^{-1} s^{-1}.

(b) As for Fig. 6a but with ω_s and shearwise tilting frontogenesis. Variables labeled, contoured, and shaded as in Fig. 6a. (c) As for Fig. 6a but with ω_n and transverse tilting frontogenesis. Variables labeled, contoured, and shaded as in Fig. 6a.

Fig. 7 (a) As for Fig. 5a but from the Eta model analysis valid at 0000 UTC 12 November 2003. Vertical cross-sections along line B-B` shown in Fig. 8. (b) As for Fig. 5b but from the Eta model analysis valid at 0000 UTC 12 November 2003. (c) As for Fig. 5c but from the Eta model analysis valid at 0000 UTC 12 November 2003.

Fig. 8 (a) Vertical cross-section along line B-B` in Fig. 7a. As for Fig. 6a but from the Eta model analysis valid at 0000 UTC 12 November 2003. (b) As for Fig. 6b but from the Eta model analysis valid at 0000 UTC 12 November 2003. (c) As for Fig. 6c but from the Eta model analysis valid at 0000 UTC 12 November 2003.

Fig. 9 (a) As for Fig. 5a but from the Eta model analysis valid at 1200 UTC 12 November 2003. Vertical cross-sections along line C-C` shown in Fig. 10. (b) As for Fig. 5b but from the Eta model analysis valid at 1200 UTC 12 November 2003. (c) As for Fig. 5c but from the Eta model analysis valid at 1200 UTC 12 November 2003.

Fig. 10 (a) Vertical cross-section along line C-C` in Fig. 9a. As for Fig. 6a but from the Eta model analysis valid at 1200 UTC 12 November 2003. Total tilting frontogenesis is contoured every 6 (-6) x 10^{-10} K m^{-1} s^{-1} beginning at 6 (-6) x 10^{-10} K m^{-1} s^{-1}. (b) As for Fig. 6b but from the Eta model analysis valid at 1200 UTC 12 November 2003. Shearwise tilting frontogenesis contoured and shaded as in Fig. 10a. (c) As for Fig. 6c but from the Eta model analysis valid at 1200 UTC 12 November 2003. Transverse tilting frontogenesis is contoured and shaded as in Fig. 10a.

Fig. 11 (a) As for Fig. 5a but from the Eta model analysis valid at 0000 UTC 13 November 2003. Vertical cross-sections along line D-D` shown in Fig. 12. (b) As for Fig. 5b but from the Eta model analysis valid at 0000 UTC 13 November 2003. (c) As for Fig. 5c but from the Eta model analysis valid at 0000 UTC 13 November 2003.

Fig. 12 (a) Vertical cross-section along line D-D` in Fig. 11a. As for Fig. 10a but from the Eta model analysis valid at 0000 UTC 13 November 2003. (b) As for Fig. 10b but from the Eta model analysis valid at 0000 UTC 13 November 2003. (c) As for Fig. 10c but from the Eta model analysis valid at 0000 UTC 13 November 2003.

Fig. 13 Schematic illustrating the mechanisms by which positive rotational frontogenesis is induced in the vicinity of an isolated vertical vorticity maxima. Dark shaded oval represents the vertical vorticity maxima. Black arrows are the associated $\boldsymbol{Q_s}$ vectors. Thin dashed lines are isentropes. Convergence (divergence) of $\boldsymbol{Q_s}$ downshear (upshear)

of the vorticity maxima is associated with ascent (descent) indicated by the thick solid (dashed) lines. Lightly shaded regions upshear and downshear of the vorticity maxima are characterized by positive rotational frontogenesis induced by along-shear tilting (i.e. $\frac{\partial \omega}{\partial s} > 0$). In the unshaded center region, $\frac{\partial \omega}{\partial s} < 0$ and positive rotational frontogenesis is forced instead by cyclonic rotation associated with the vertical vorticity maxima. See text for additional explanation.

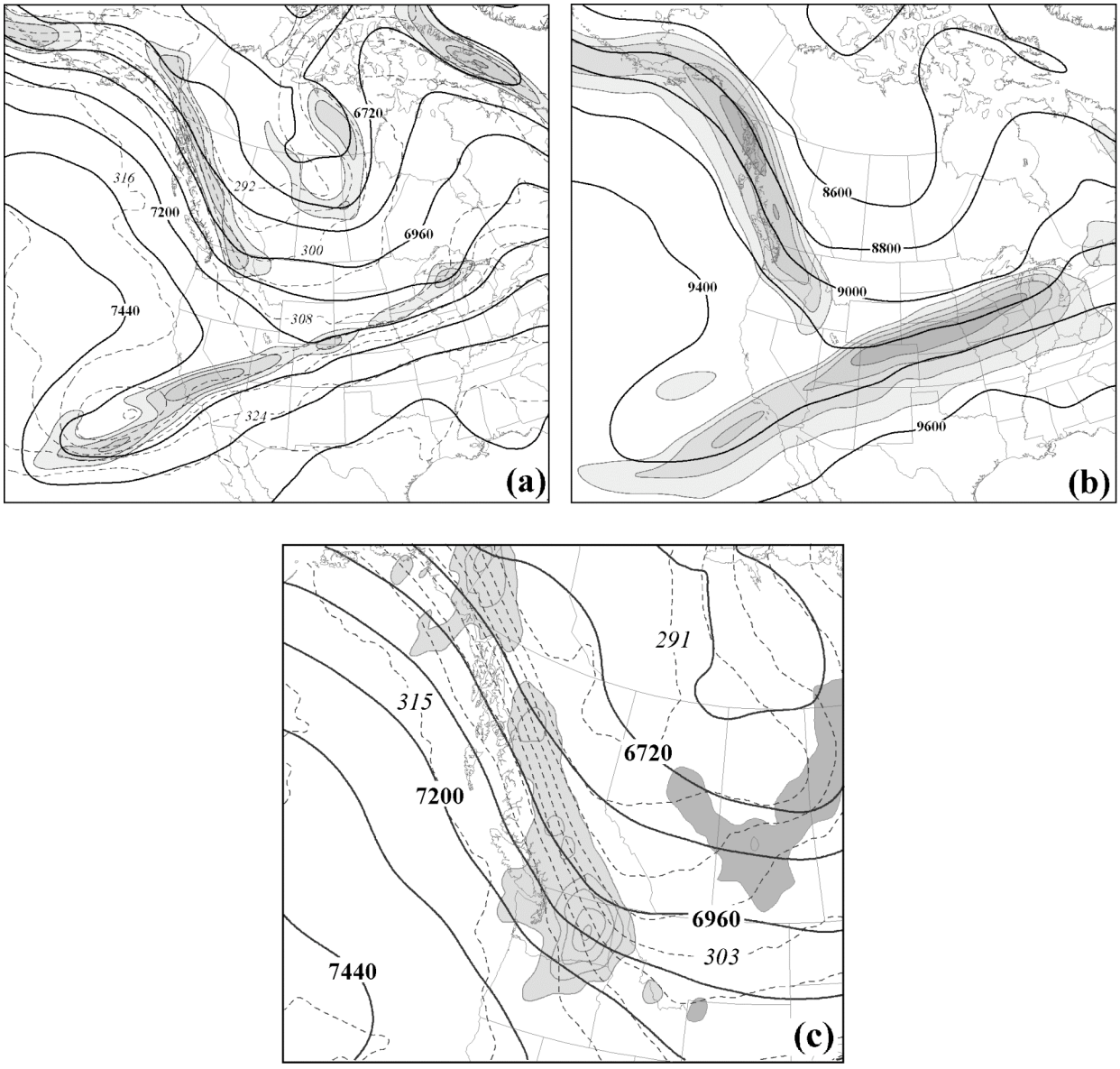

Fig. 1 (a) 400 hPa geopotential height (solid lines), potential temperature (dashed) and absolute vorticity (shading) from the Eta model analysis valid at 1200 UTC 11 November 2003. Geopotential height is labeled in m and contoured every 120 m. Isentropes are labeled in K and contoured every 4 K. Absolute vorticity shown in units of 10^{-5} s^{-1} and shaded every 5 x 10^{-5} s^{-1} beginning at 15 x 10^{-5} s^{-1} (b) 300 hPa geopotential height (solid lines) and isotachs (shaded) from the Eta model analysis valid at 1200 UTC 11 November 2003. Geopotential height labeled as in Fig. 1a and contoured every 200 m. Isotachs shown in m s^{-1} and shaded every 10 m s^{-1} beginning at 40 m s^{-1}. (c) 400 hPa geopotential height (solid lines), isentropes (dashed lines) and geostrophic temperature advection (shading) from the Eta model analysis valid at 1200 UTC 11 November 2003. Geopotential height labeled and contoured as in Fig. 1a. Isentropes labeled in K and contoured every 3K. Dark (light) shading represents negative (positive) geostrophic temperature advection in units of K s^{-1}, contoured every – 2 (2) x 10^{-4} K s^{-1} beginning at – 2 (2) x 10^{-4} K s^{-1}.

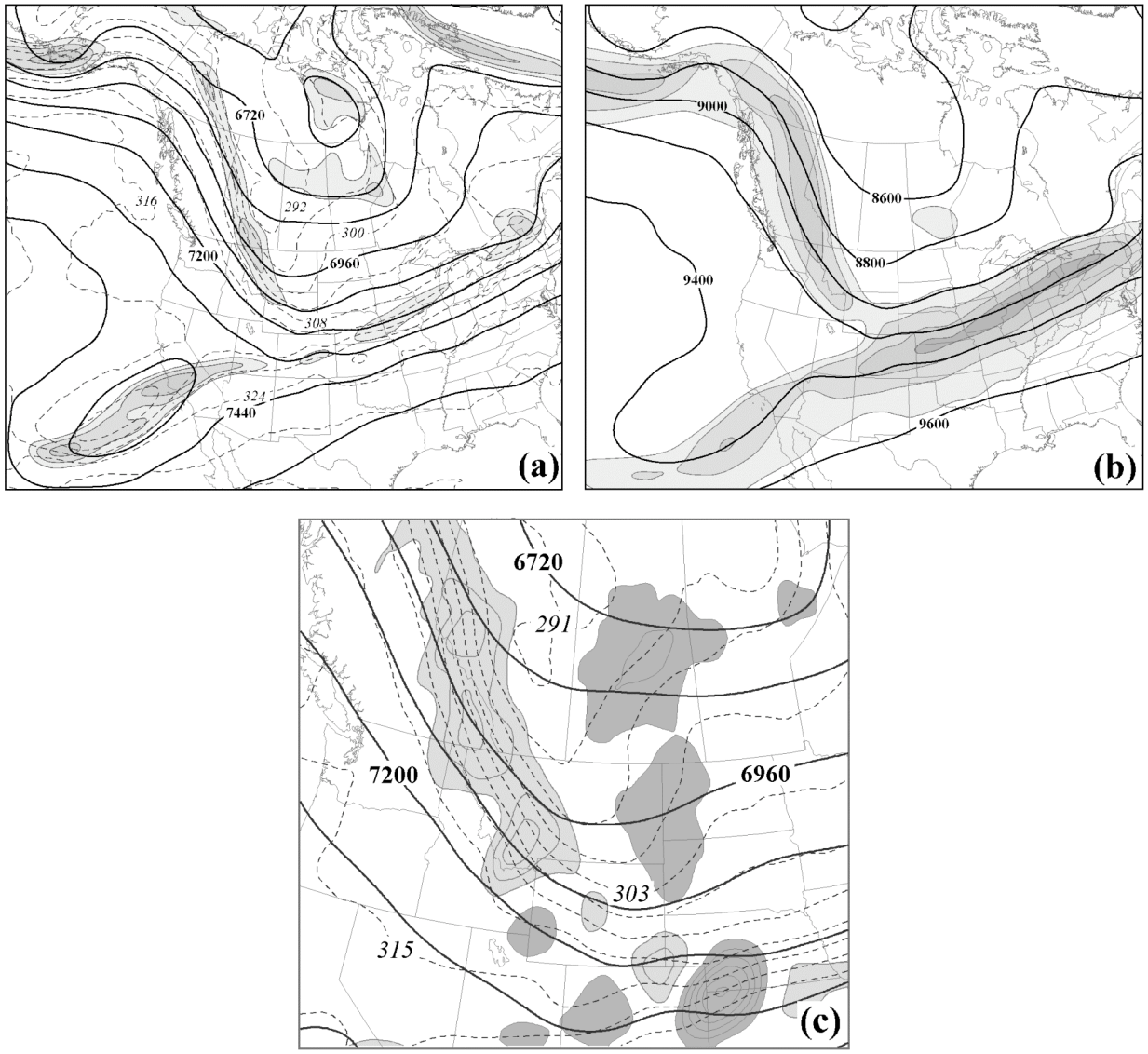

Fig. 2 (a) As for Fig. 1a but from the Eta model analysis valid at 0000 UTC 12 November 2003. (b) As for Fig. 1b but from the Eta model analysis valid at 0000 UTC 12 November 2003. (c) As for Fig. 1c but from the Eta model analysis valid at 0000 UTC 12 November 2003.

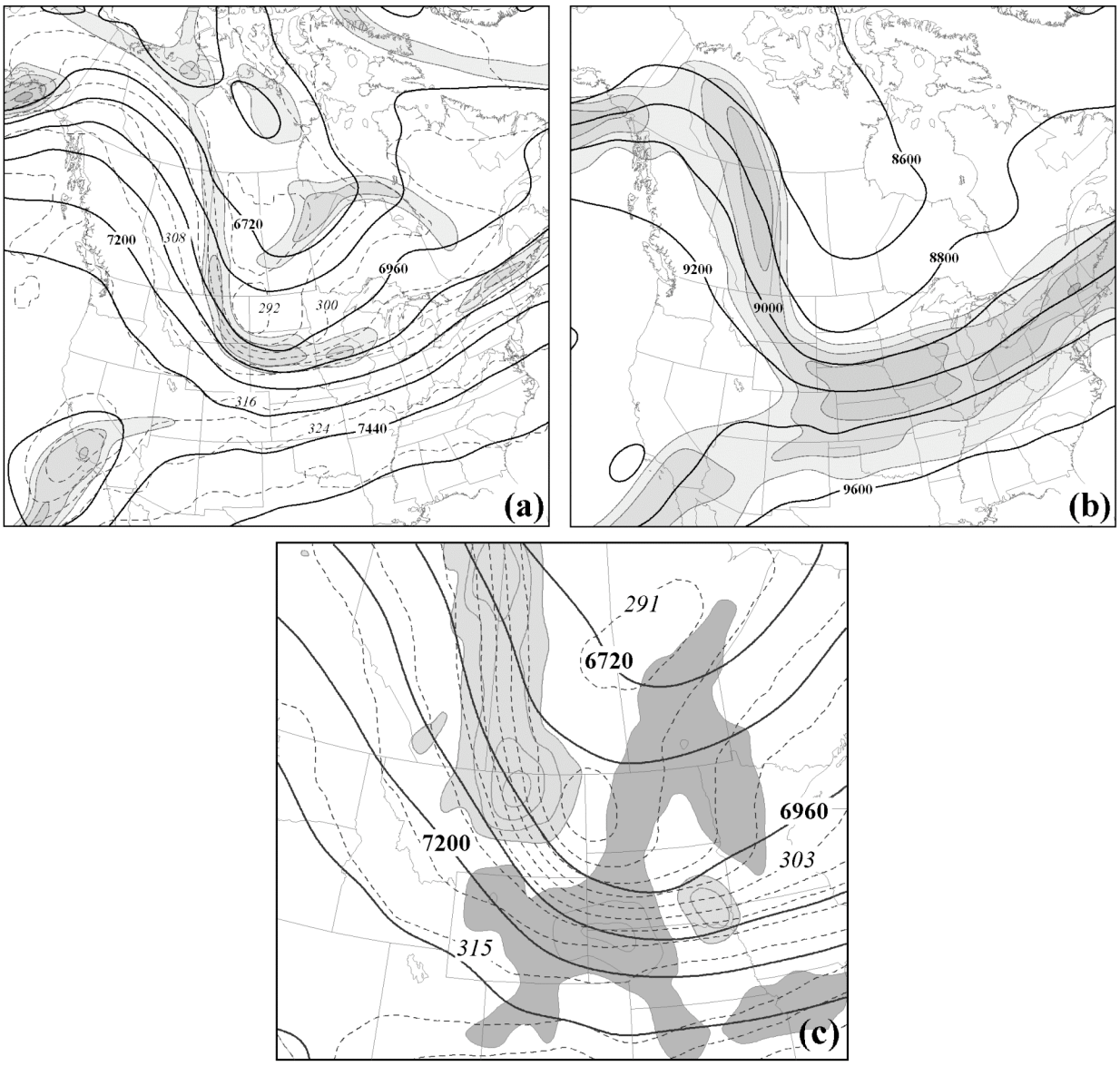

Fig. 3 (a) As for Fig. 1a but from the Eta model analysis valid at 1200 UTC 12 November 2003. (b) As for Fig. 1b but from the Eta model analysis valid at 1200 UTC 12 November 2003. (c) As for Fig. 1c but from the Eta model analysis valid at 1200 UTC 12 November 2003.

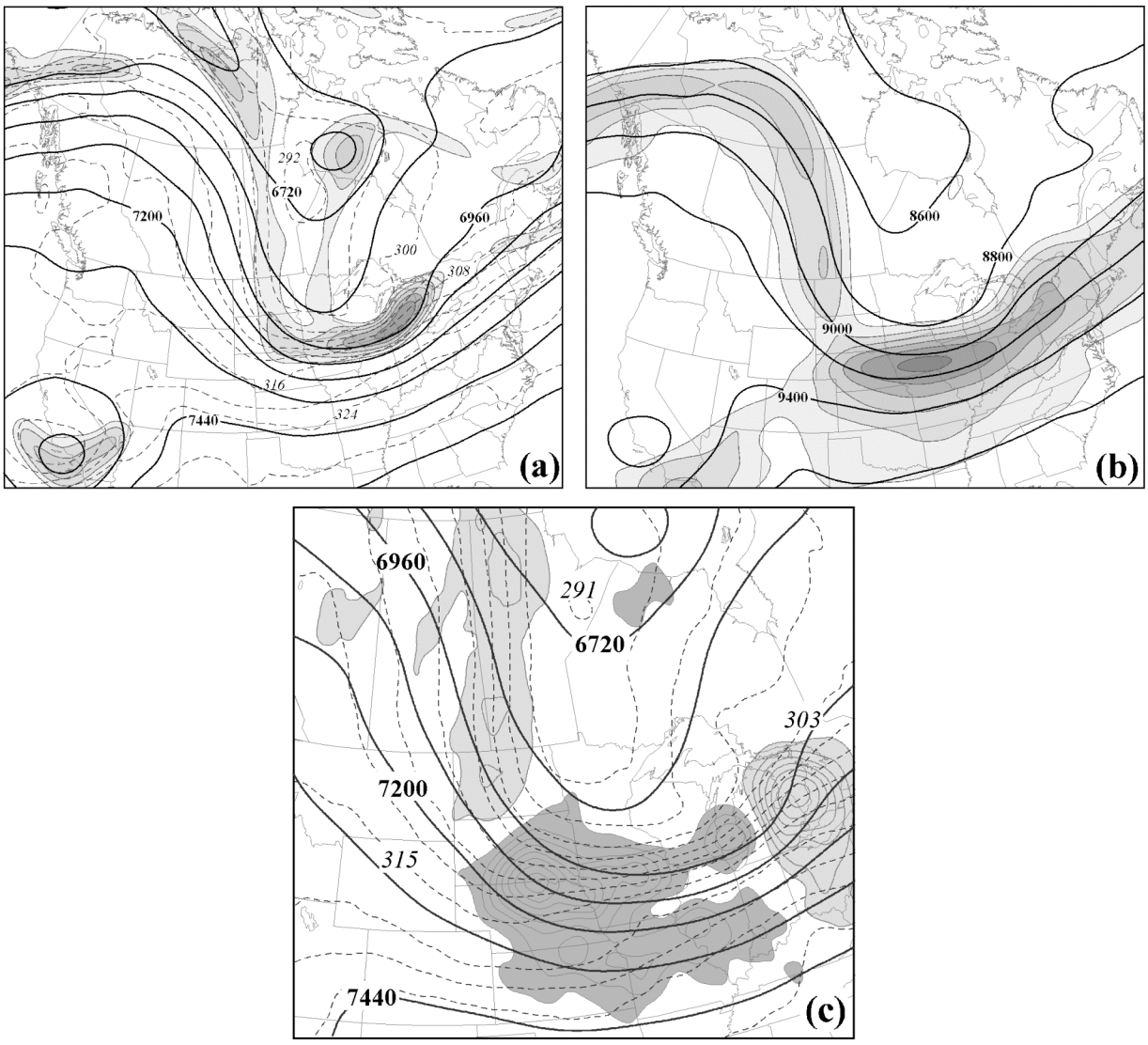

Fig. 4 (a) As for Fig. 1a but from the Eta model analysis valid at 0000 UTC 13 November 2003. (b) As for Fig. 1b but from the Eta model analysis valid at 0000 UTC 13 November 2003. (c) As for Fig. 1c but from the Eta model analysis valid at 0000 UTC 13 November 2003.

Fig. 5 (a) 400 hPa isentropes, ***Q***-vectors, total QG vertical motions (ω_{tot}), and tilting frontogenesis calculated using ω_{tot} from the Eta model analysis valid at 1200 UTC 11 November 2003. Thin solid lines are isentropes, labeled in K and contoured every 3K. Thick solid (dashed) lines are positive (negative) ω_{tot} contoured every 2 (-2) dPa s^{-1} beginning at 2 (-2) dPa s^{-1}. Tilting frontogenesis is in units of K m^{-1} s^{-1} and contoured every 8 (-8) x 10^{-10} K m^{-1} s^{-1} starting at 8 (-8) x 10^{-10} K m^{-1} s^{-1} with dark (light) shading indicating positive (negative) tilting frontogenesis. Vertical cross-sections along line A-A` shown in Fig. 6. (b) As for Fig. 5a but with $\boldsymbol{Q_s}$ vectors, shearwise QG vertical motions (ω_s), and shearwise tilting frontogenesis from the Eta model analysis valid at 1200 UTC 11 November 2003. Tilting frontogenesis contoured in units of 4 (-4) x 10^{-10} K m^{-1} s^{-1} beginning at 4 (-4) x 10^{-10} K m^{-1} s^{-1}. (c) As for Fig. 5a but with $\boldsymbol{Q_n}$ vectors, transverse QG vertical motions (ω_n), and transverse tilting frontogenesis from the Eta model analysis valid at 1200 UTC 11 November 2003. Tilting frontogenesis contoured and shaded as in Fig. 5b.

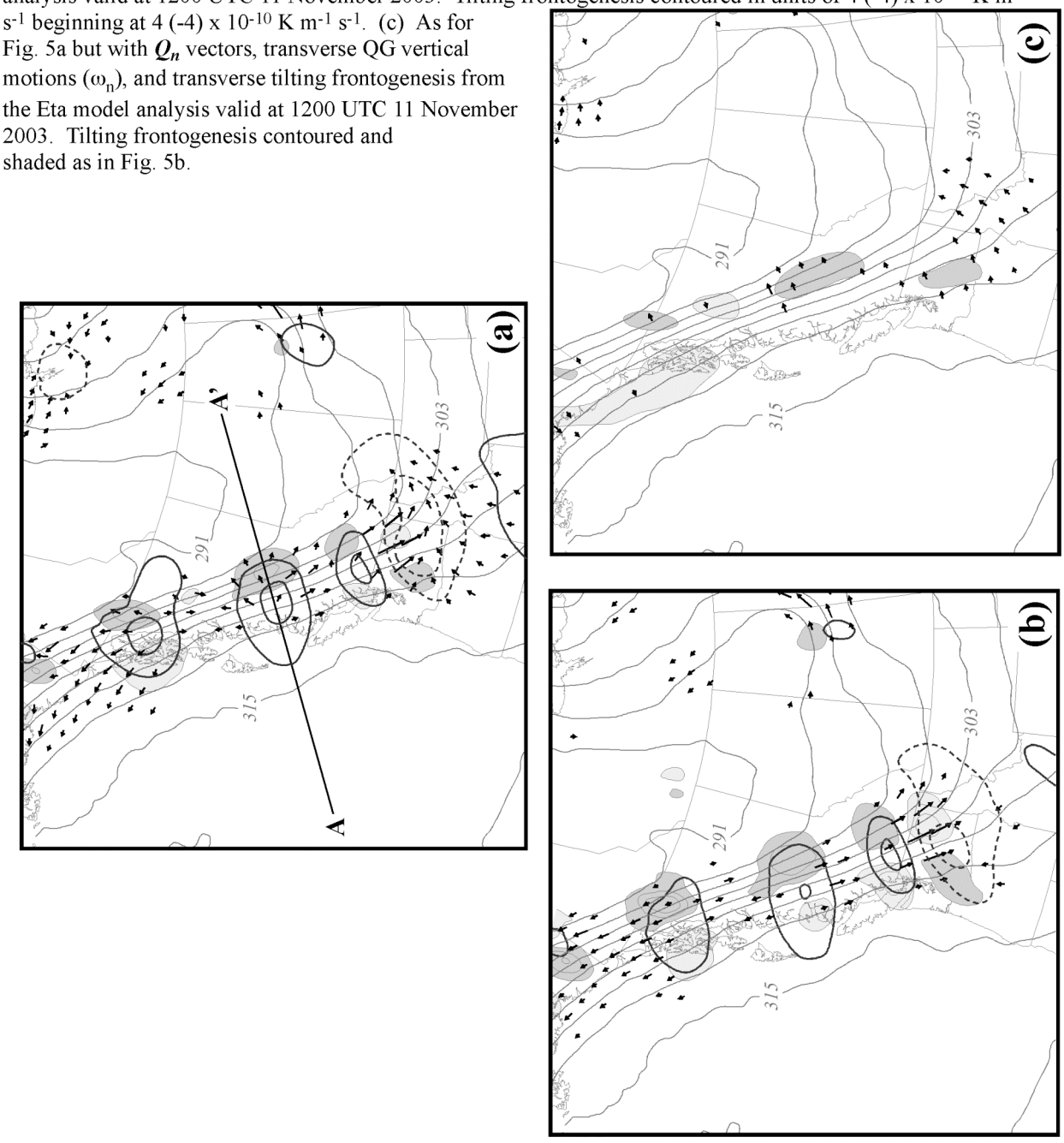

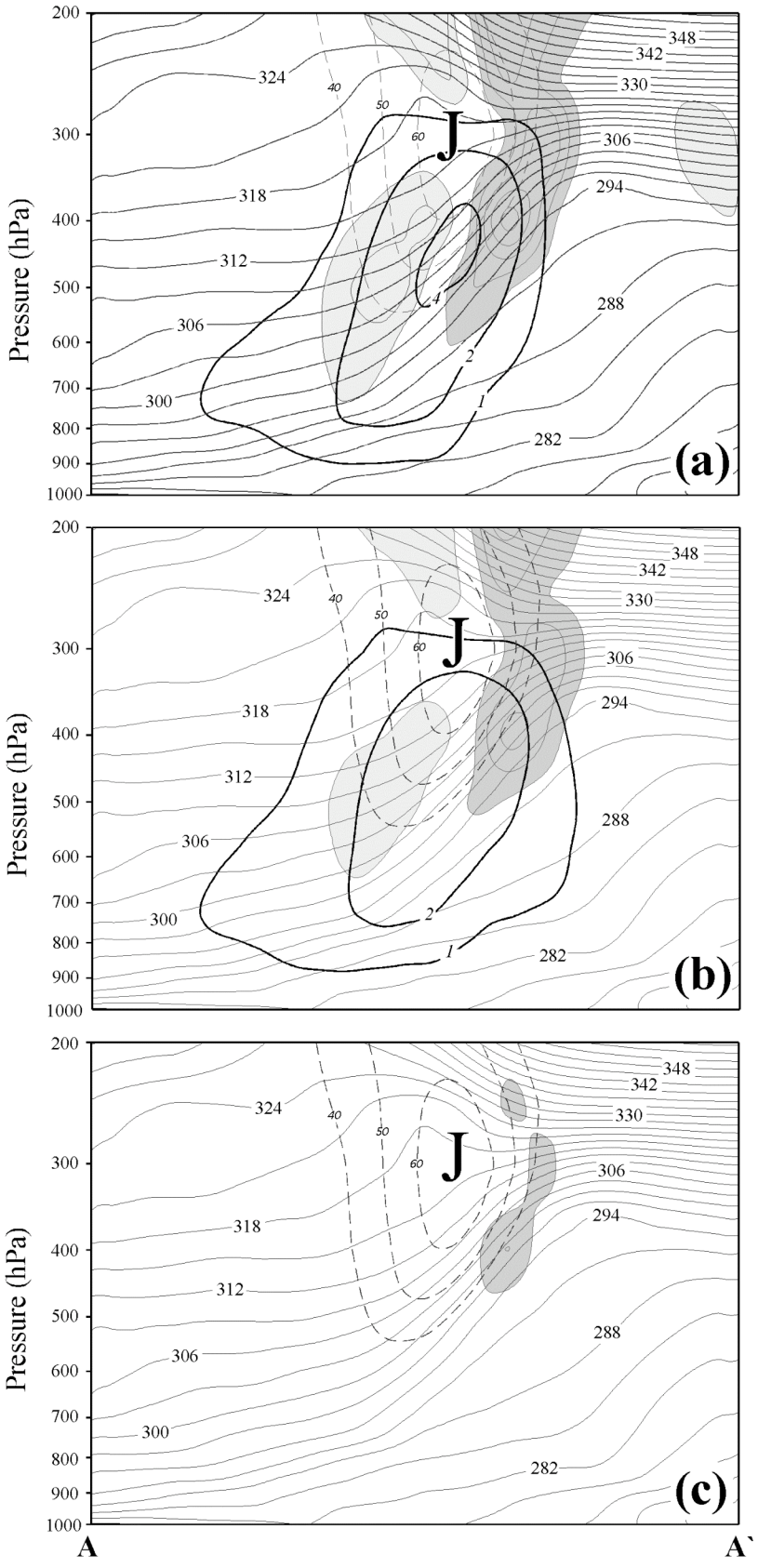

Fig. 6 (a) Vertical cross section, along line A-A` in Fig. 5a, of isotachs, isentropes, ω_{tot}, and total tilting frontogenesis from the Eta model analysis valid at 1200 UTC 11 November 2003. Thin dashed lines are isotachs labeled in m s^{-1} and contoured every 10 m s^{-1} starting at 40 m s^{-1}. Uppercase " J" indicates the location of the jet core. Isentropes labeled and contoured as in Fig. 5a. Thick solid (dashed) lines are positive (negative) ω_{tot} labeled in dPa s^{-1} and contoured every 2 (-2) dPa s^{-1} beginning at 2 (-2) dPa s^{-1} but including the 1 (-1) dPa s^{-1} contour as well. Positive (negative) tilting frontogenesis is darkly (lightly) shaded and contoured every 3 (-3) x 10^{-10} K m^{-1} s^{-1} beginning at 3 (-3) x 10^{-10} K m^{-1} s^{-1}. (b) As for Fig. 6a but with ω_s and shearwise tilting frontogenesis. Variables labeled, contoured, and shaded as in Fig. 6a. (c) As for Fig. 6a but with ω_n and transverse tilting frontogenesis, Variables labeled, contoured, and shaded as in Fig. 6a.

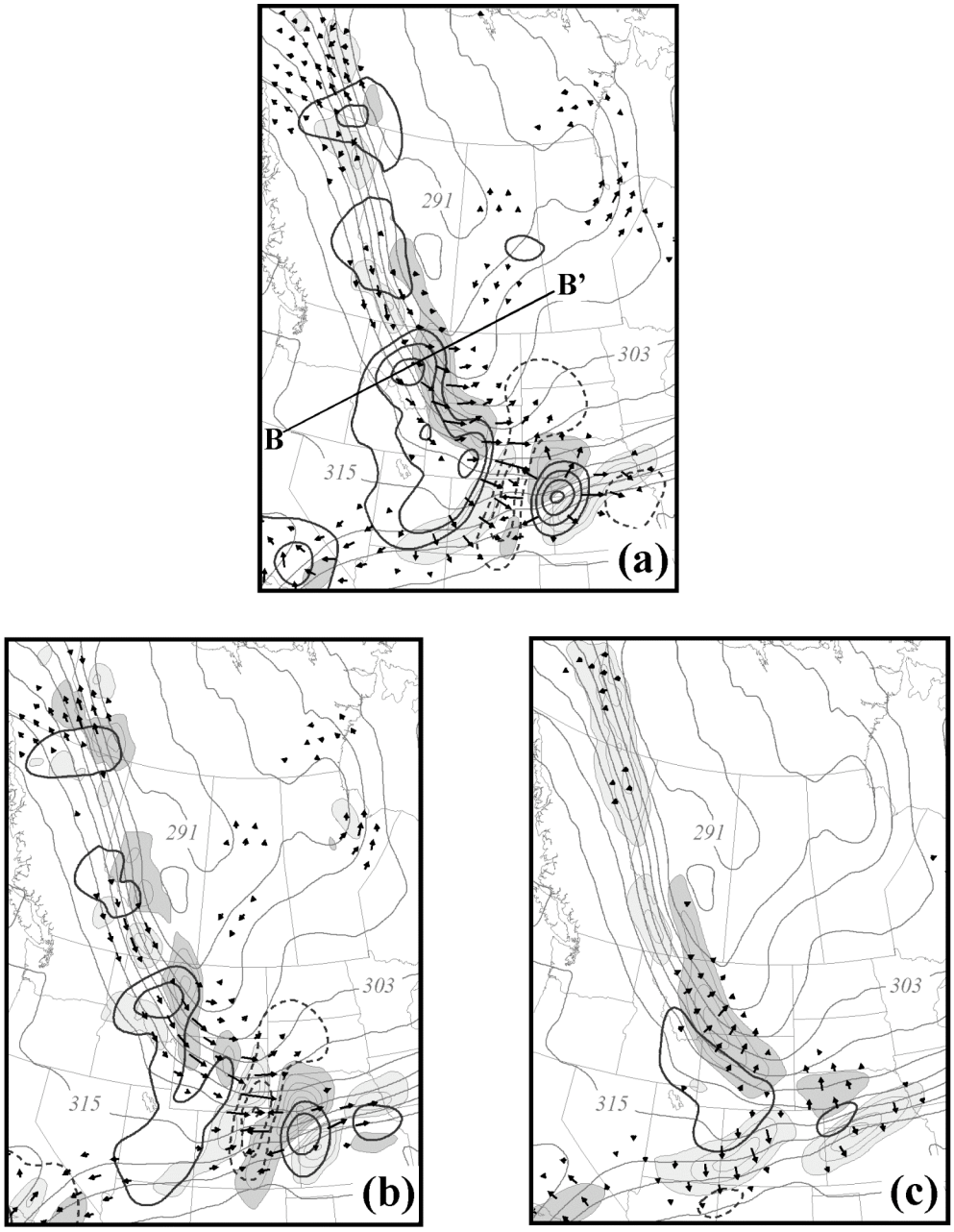

Fig. 7 (a) As for Fig. 5a but from the Eta model analysis valid at 0000 UTC 12 November 2003. Vertical cross-sections along line B-B` shown in Fig. 8. (b) As for Fig. 5b but from the Eta model analysis valid at 0000 UTC 12 November 2003. (c) As for Fig. 5c but from the Eta model analysis valid at 0000 UTC 12 November 2003.

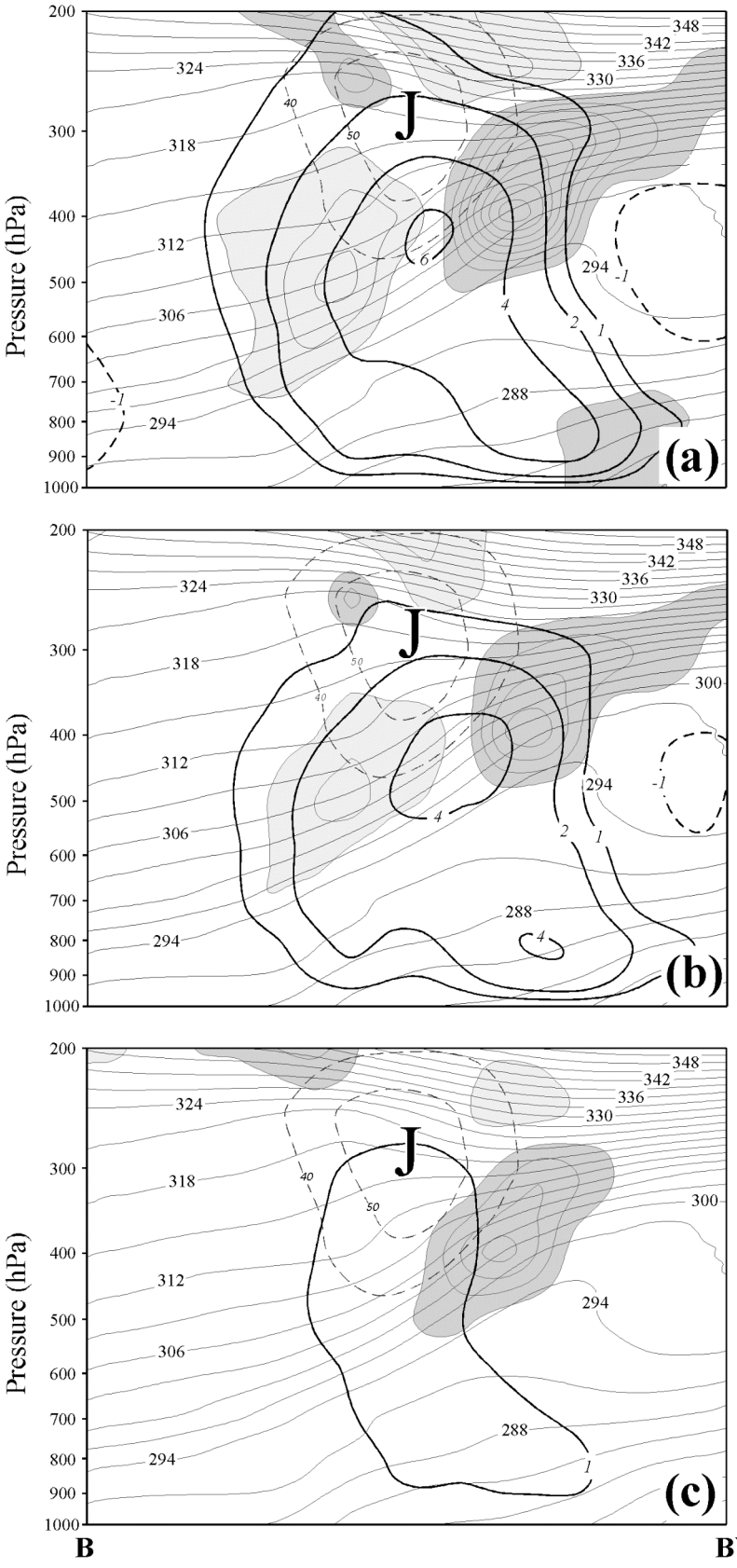

Fig. 8 (a) Vertical cross-section along line B-B` in Fig. 7a. As for Fig. 6a but from the Eta model analysis valid at 0000 UTC 12 November 2003. (b) As for Fig. 6b but from the Eta model analysis valid at 0000 UTC 12 November 2003. (c) As for Fig. 6c but from the Eta model analysis valid at 0000 UTC 12 November 2003.

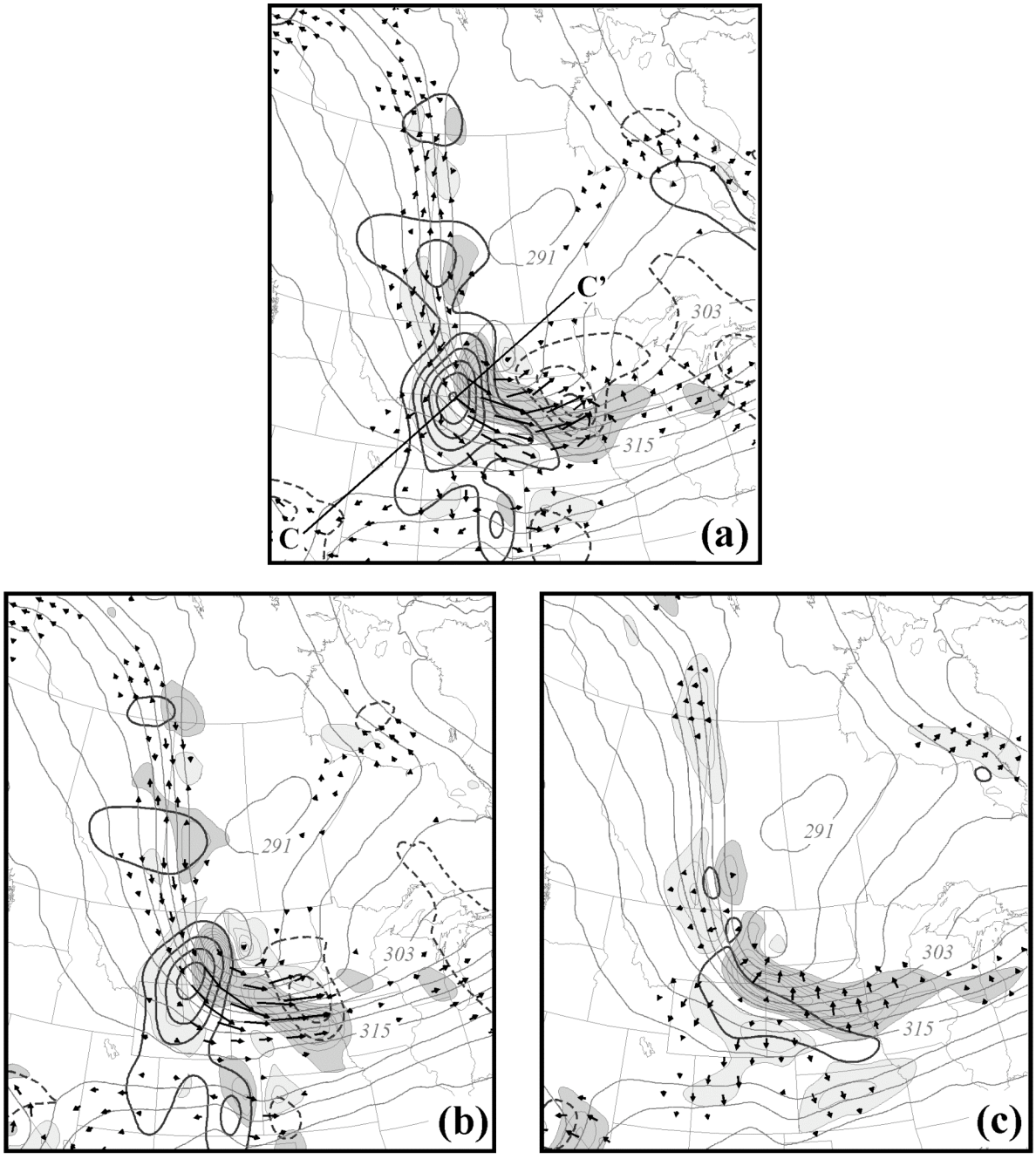

Fig. 9 (a) As for Fig. 5a but from the Eta model analysis valid at 1200 UTC 12 November 2003. Vertical cross-sections along line C-C` shown in Fig. 10. (b) As for Fig. 5b but from the Eta model analysis valid at 1200 UTC 12 November 2003. (c) As for Fig. 5c but from the Eta model analysis valid at 1200 UTC 12 November 2003.

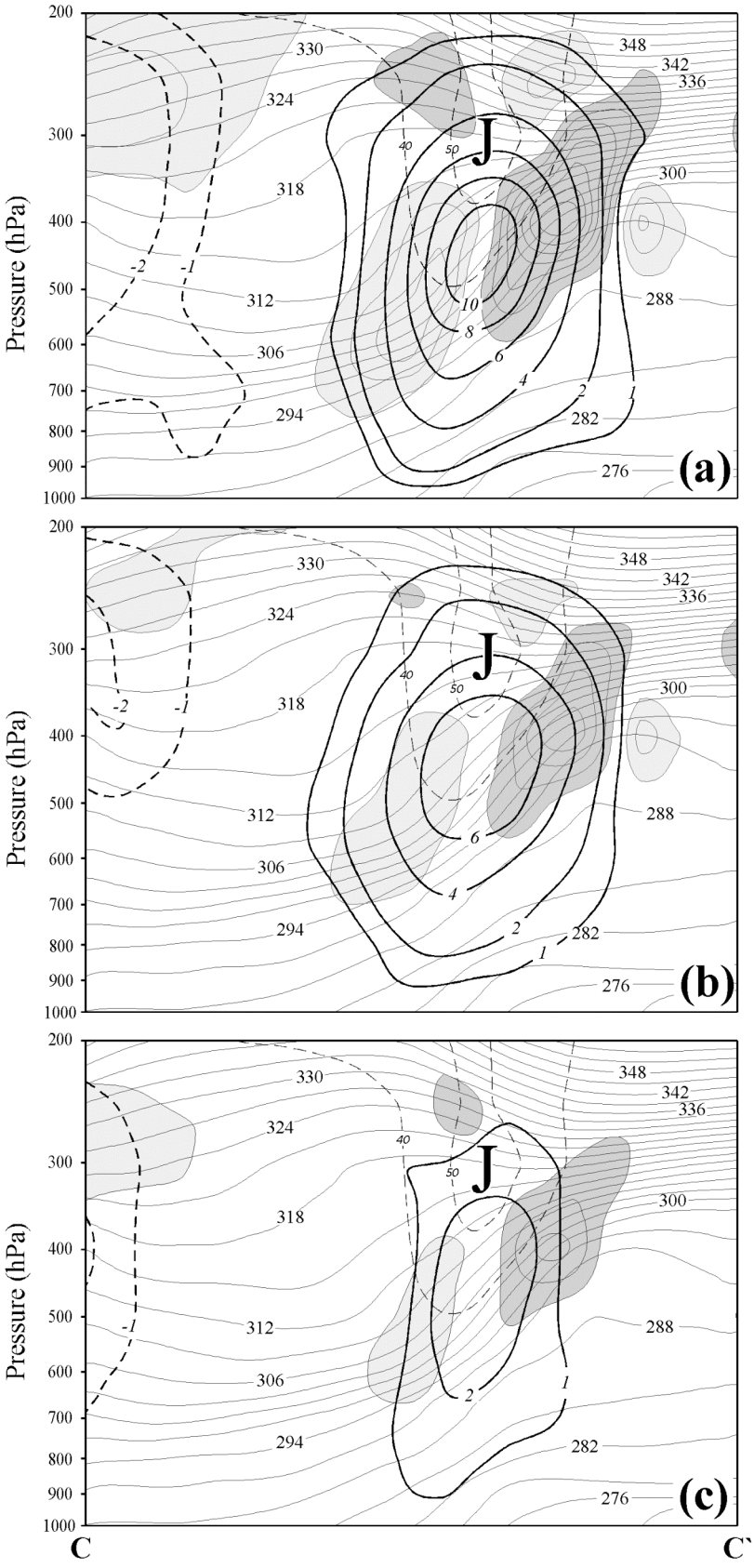

Fig. 10 (a) Vertical cross-section along line C-C` in Fig. 9a. As for Fig. 6a but from the Eta model analysis valid at 1200 UTC 12 November 2003. Tilting frontogenesis is contoured every 6 (-6) x 10^{-10} K m^{-1} s^{-1} beginning at 6 (-6) x 10^{-10} K m^{-1} s^{-1}. (b) As for Fig. 6b but from the Eta model analysis valid at 1200 UTC 12 November 2003. Tilting frontogenesis contoured and shaded as in Fig. 10a. (c) As for Fig. 6c but from the Eta model analysis valid at 1200 UTC 12 November 2003. Tilting frontogenesis is contoured and shaded as in Fig. 10a.

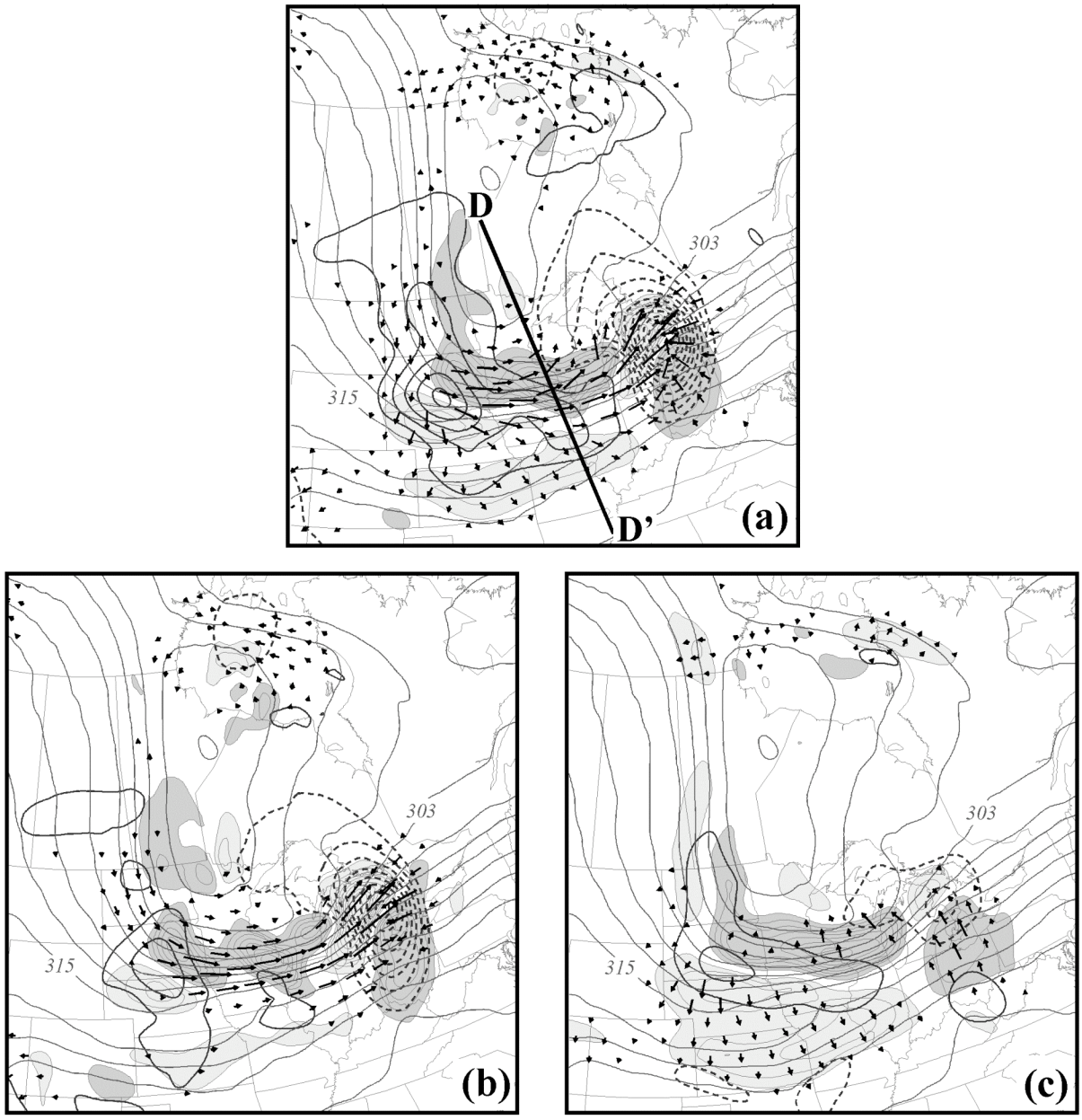

Fig. 11 (a) As for Fig. 5a but from the Eta model analysis valid at 0000 UTC 13 November 2003. Vertical cross sections along line D-D` shown in Fig. 12. (b) As for Fig. 5b but from the Eta model analysis valid at 0000 UTC 13 November 2003. (c) As for Fig. 5c but from the Eta model analysis valid at 0000 UTC 13 November 2003.

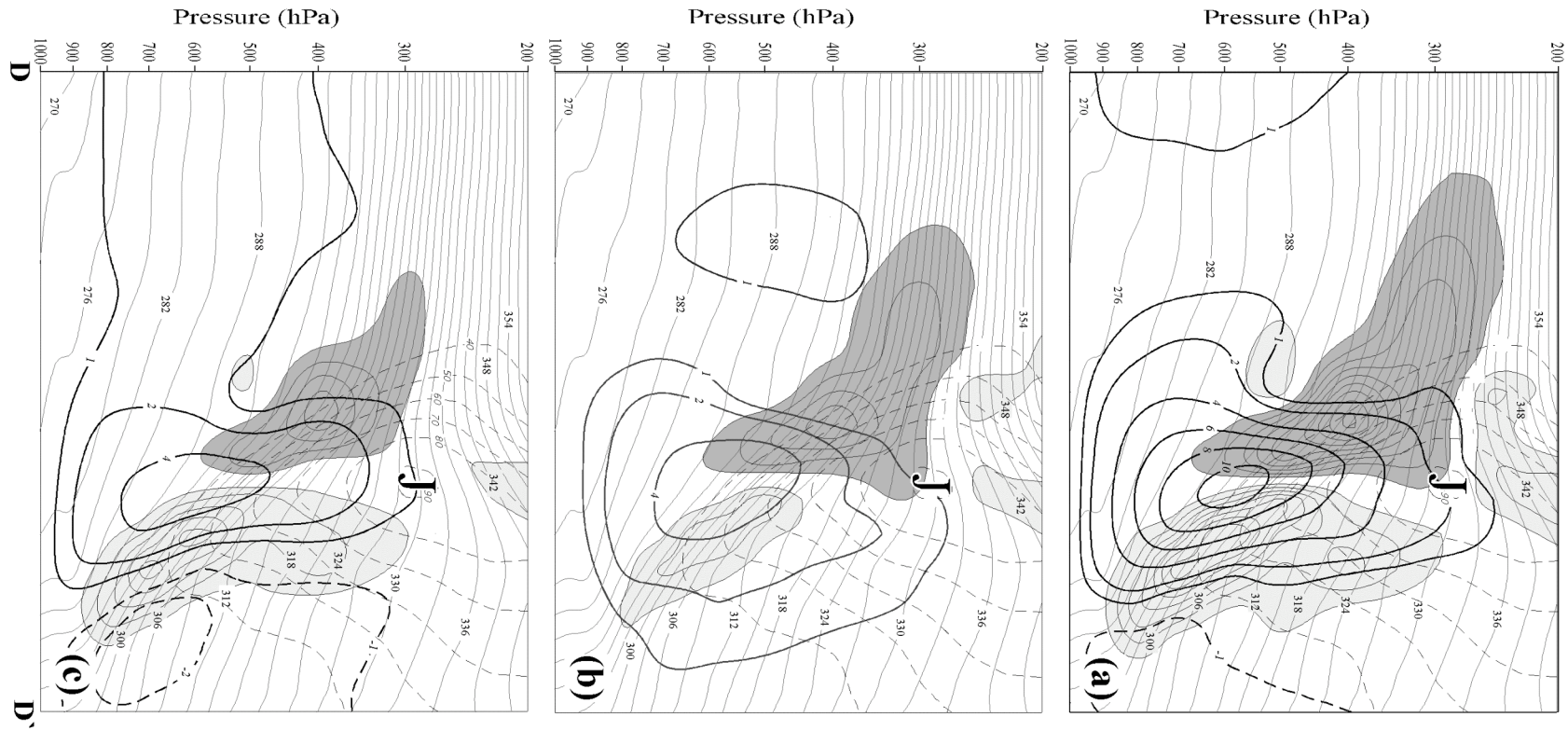

Fig. 12 (a) Vertical cross-section along line D-D` in Fig. 11a. As for Fig. 6a but from the Eta model analysis valid at 0000 UTC 13 November 2003. Tilting frontogenesis is contoured every 6 (-6) x 10^{-9} K m^{-1} s^{-1} beginning at 6 (-6) x 10^{-9} K m^{-1} s^{-1}. (b) As for Fig. 6b but from the Eta model analysis valid at 0000 UTC 13 November 2003. Tilting frontogenesis contoured and shaded as in Fig. 12a. (c) As for Fig. 6c but from the Eta model analysis valid at 0000 UTC 13 November 2003. Tilting frontogenesis is contoured and shaded as in Fig. 12a.

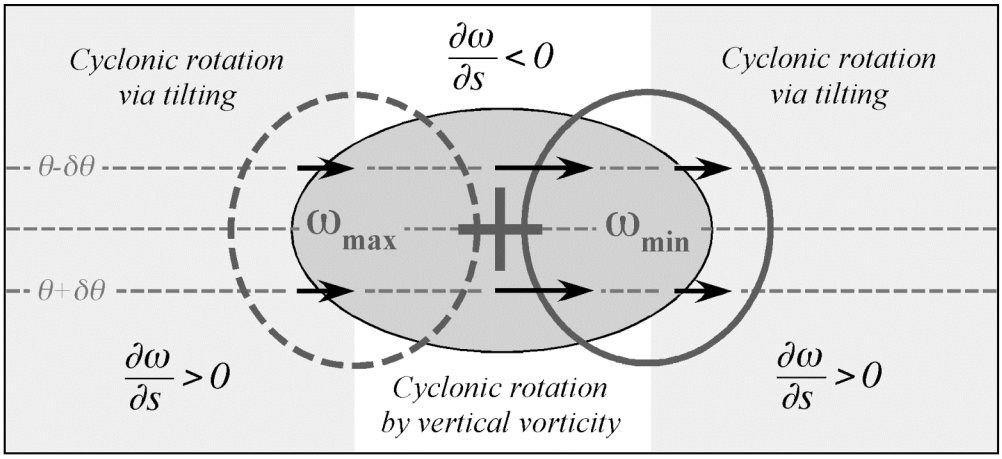

Fig. 13 Schematic illustrating the mechanisms by which positive rotational frontogenesis is induced in the vicinity of an isolated vertical vorticity maxima. Dark shaded oval represents the vertical vorticity maxima. Black arrows are the associated $\boldsymbol{Q_s}$ vectors. Thin dashed lines are isentropes. Convergence (divergence) of $\boldsymbol{Q_s}$ downshear (upshear) of the vorticity maxima is associated with ascent (descent) indicated by the thick solid (dashed) lines. Lightly shaded regions upshear and downshear of the vorticity maxima are characterized by positive rotational frontogenesis induced by along-shear tilting (i.e. $\frac{\partial \omega}{\partial s} > 0$). In the unshaded center region, $\frac{\partial \omega}{\partial s} < 0$ and positive rotational frontogenesis is forced instead by cyclonic rotation associated with the vertical vorticity maxima. See text for additional explanation.